第 35 卷第 5 期
2019 年 5 月

无 机 化 学 学 报
CHINESE JOURNAL OF INORGANIC CHEMISTRY

Vol.35 No.5
891-900

羟基磷灰石负载放射性 ^{18}F 作为分子影像纳米探针在生物医学中的应用

吴 睿* 卢久富 宋 娟 刘存芳 张 强 田光辉*

(陕西理工大学化学与环境科学学院,陕西省催化基础与应用重点实验室,汉中 723001)

摘要:采用简便有效的方法,制备了生物兼容性强、放射性标记羟基磷灰石(HAp)纳米粒子的正电子发射计算机断层显像(PET)纳米探针。在合成 HAp 纳米粒子的过程中,放射性的 ^{18}F 作为掺杂剂,占据 HAp 晶格中羟基位置,在短时间内牢固地标记到 HAp 上。^{18}F 不仅标记在纳米粒子的表面,而且还通过强的化学键标记在纳米颗粒的内部。以达到提高标记量并防止辐射泄漏的目的。设计的高标记量的放射性纳米探针应用于动物实验并靶向到达脏器器官。

关键词:羟基磷灰石;放射性标记;掺杂;^{18}F

中图分类号:O615.4+5 **文献标识码**:A **文章编号**:1001-4861(2019)05-0891-10

DOI:10.11862/CJIC.2019.120

Hydroxyapatite Loaded Radiolabeled ^{18}F as Molecular Imaging Nanoprobes for Biomedical Application

WU Rui* LU Jiu-Fu SONG Juan LIU Cun-Fang ZHANG Qiang TIAN Guang-Hui*

(*Shaanxi Key Laboratory of Catalysis, College of Chemical & Environment Science, Shaanxi University of Technology, Hanzhong, Shaanxi* 723001, *China*)

Abstract: Biocompatible and radiolabeled hydroxyapatite nanoparticles (HAp NPs) as positron emission tomography (PET) nanoprobes were developed by a facile and effective method. Radioactive ^{18}F was firmly incorporated in the process of synthesis HAp as dopant by occupying hydroxyl vacancy in lattice of HAp in a short time. ^{18}F was not only on the surface of the HAp NPs but also inner by strong chemical bond to achieve the purpose of large amounts of labelling and prevent radiation leakage. The designed high load of radiolabeled HAp NPs was applied to animal experiment and targeted to viscera organs.

Keywords: hydroxyapatite; radiolabeled; doping; ^{18}F

0 Introduction

Molecular or personalized medicine is the future of patient management and molecular imaging plays a key role in healthy. Molecular imaging refers to the characterization and measurement of biological processes at the molecular or cellular level[1-4]. Recently, the emergence of novel nanoprobes for molecular imaging was employed for earlier disease detection[5-7]. One of the most primary goal in molecular imaging is to obtain high signal and localize the signal as accurately as possible with high temporal resolution and with minimal amount of molecular probe, namely achieving higher contrast ratio of the imaging. In

收稿日期:2018-11-01。收修改稿日期:2019-03-22。

陕西省自然科学基金(No.2018JQ2057),陕西省教育厅科研计划(No.17JK0151),陕西理工大学博士研究基础项目(No.209020195),国家自然科学基金(No.21502109)和陕西省教育厅重点科研项目(No.18JS023,17JS027)资助。

*通信联系人。E-mail:hftffc@163.com

keeping pace with these milestones in the evolution of medical imaging, there is no doubt that PET is the most high sensitive and accurate molecular imaging modality, which has the potential to revolutionize diagnostics and therapeutic monitoring in clinic [8-10]. But it remains imperative to develop higher sensitivity imaging method for clinical practice. At present, most of the researchers for PET worldwide perform in oncologic patients, by using FDG (fluorodeoxy glucose) and it′s derivative, as well as some NPs for ^{18}F carrier[11-19]. Despite its high diagnostic accuracy in the important role of determining the neoplasm, PET is expected to play a pivotal role for more and more disease as a relatively well entrenched diagnostic tool.

However, for the most part, these advances have not translated into greatly improved clinical outcomes. The reason for this is that each [^{18}F]FDG can only carried one ^{18}F that trapped the development of [^{18}F] FDG probes as higher contrast agent. Furthermore, it cannot differentiate between cancer and inflammation in diagnosis of the tumor. Advances in PET for tumor are now extending the application further into lymphatic imaging. Success in these endeavors requires a new effort in many innovations.

In view of this, it is reasonable to assume that if we can study on innovation for the challenge above, the PET imaging may come true. Nanomedicine may has the potential to provide novel and paradigm shifting solution for the challenge. It is supposed that radionuclides were doped in the process of synthesis trace amount of nanoprobes. As a result, large number of radionuclides were labeled in the nanoparticles and the efficient signal enhanced as well as other advantages. Furthermore, the radionuclides were trapped in the NPs avoiding leakage and the large surface of the NPs was used for other purposes.

To reach the goal, three protagonists are mandatory. One of the top priorities is the synthesis methods that its fate is of paramount importance to ensure trace synthesis due to the limited radionuclide produced in cyclotron. A second issue is the modification on the surface in a short time. In line with this, the third concern is the sophisticated techniques and methods of separation and purification in a short time.

^{18}F is the most readily available and widely used in PET due to its favorable half-life of 110 min and its ease of production in cyclotron. Therefore, they are utilizable by a high number of PET centers in hospital. HAp is calcium phosphate compound with the chemical formula $Ca_{10}(PO_4)_6(OH)_2$. Owing to their low toxicity, good biocompatibility, HAp NPs were applied in cell labeling, tracking, imaging, drug delivery[20-23].

Herein, in recognition of this, we open our mind to the widening field of the PET outside the FDG kingdom. A thorough and fascinating study is meet to the expected nanoprobes above. In previous report, the ^{18}F was labeled by weak physical adsorption on the surface of HAp NPs[24-25]. Due to dopping ^{18}F in the process of synthesis in trace amount, ^{18}F was not only strong tied to the surface but also was inside by strong chemical covalent bond. In line with this, due to the present of the limited resources of ^{18}F and the trace amount of HAp, each HAp NP carried large amount of ^{18}F. So the detection signal will be strong enough. In addition, because of the lager volume of HAp NPs inside than outside, overwhelming majority of ^{18}F were encapsulated which were relative safe to human body. It is expected that the safe, green and efficient nanoprobes will provide an interesting platform for developing biochemistry and biomedicine.

1 Experimental

1.1 Chemicals

Disodium hydrogen phosphate, diammonium hydrogen phosphate, calcium nitrate, sodium dihydrogen phosphate and ammonium hydroxide were obtained from Sinopharm Chemical Reagent Co., Ltd. The pentobarbital sodium was purchased from Sigma-Aldrich. Hexadecyl (cetyl) trimethyl ammonium bromide (CTAB), sodium citrate (Na-Cit) and polyethylene glycol (PEG) were purchased from Tianjin Fu-chen Chemical Reagent Science and Technology Co., Ltd. All chemicals were analysis-grade. All water was deionized.

1.2 Synthesis of HAp NPs and doping of ^{19}F

Chemical precipitation was employed to synthesize large amount of HAp NPs. Diammonium hydrogen phosphate and calcium nitrate tetrahydrate were employed as the precursors in a molar ratio of Ca to P being 1.67. Briefly, 3 mL of 0.10 mmol·L^{-1} diammonium hydrogen phosphate solution was added into 10 mL of the centrifuge tube and 5 mL of 0.10 mmol·L^{-1} calcium nitrate was dropped into the solution. The pH value of the solutions was maintained at 9~10 by adding ammonium hydroxide. The mixed solution was heated at 80 ℃ for 1h under magnetic stirring. After that, the suspension was centrifugation (24 000 r·min^{-1}) for 10 min, and washed three times with deionized water. For doping fluoride, 1 mL of 0.10 mmol·L^{-1} sodium fluoride was added to the solution, other steps are the same. The control experiments were carried out in the presence of PEG, Na-Cit and CTAB as modifier, following the same procedure. For trace amount of synthesis, 30 μL of 0.10 mmol·L^{-1} diammonium hydrogen phosphate solution participated in the reaction, the quantity of sodium fluoride remain the same, the other based on the stoichiometric ratio.

1.3 Characterization of HA NPs with TEM and EDS

The morphology and structure of the as-synthesized HAp NPs were determined by transmission electron microscope (TEM). TEM images were recorded using FEI Tecnai G2 S-Twin type with a field emission gun operating at 200 kV. EDS (energy dispersive spectrometer) was used to confirm the HAp NPs with F element.

1.4 *In vitro* stability studies

The stability of ^{18}F labeled HAp NPs (^{18}F-HAp) *in vitro* was investigated to determine the leaching of fluorine. Considering the harm of radioactive ^{18}F, the common ^{19}F replaced ^{18}F. The ^{19}F-HAp NPs were incubated in PBS (phosphate-buffered saline). The ^{19}F-HAp NPs in the presence of CTAB and without CTAB were suspended in 1 mL of PBS (pH~7.4) at 37 ℃ for 2 h. After 2 h, the NPs were characterized with TEM to check whether the morphology changed.

1.5 Synthesis of ^{18}F-HAp

^{18}F was produced by irradiation of $^{18}O^-$ water with protons from cyclotron. The solution in $^{18}O^-$ water was used without further purification. The ^{18}F was nominally in the form of no-carrier-added fluoride ions, although typically ^{19}F was also present in traces. Initial studies were performed using HAp NPs, and focused on testing the optimal medium in which to carry out the radiolabeling and optimal incubation times required. Briefly, 30 μL of 0.10 mmol·L^{-1} diammonium hydrogen phosphate solution was added into 5 mL of the centrifuge tube. Then, 1.11×10^8 Bq of ^{18}F was added to the solution, and 50 μL of 0.10 mmol·L^{-1} calcium nitrate was dropped into the solution. The pH value of the solution was maintained at 9 ~10 by sodium hydroxide. The mixed solution was heated at 80 ℃ for 1 h under magnetic stirring.

1.6 Determination of radiolabeling yield

Subsequently, radiolabeling of HAp NPs was investigated in detail. The radiolabeling yield of ^{18}F-HAp was determined by measuring the radioactive activity. PBS was added to ^{18}F-HAp solution and 5 μm of aluminum oxide powder were employed to remove free ^{18}F, filtration with 0.22 μm of membrane. Subsequently, the filter liquor was carefully pipetted out into a test tube and ^{18}F activity was measured. ^{18}F associated with HAp NPs was also measured.

1.7 Biodistribution studies

Furthermore, practical application of ^{18}F-HAp as radiotracer was investigated by biodistribution carried out in normal rats. For distribution studies, ^{18}F-HAp were injected into rats and free ^{18}F ions as control group. The animals were anesthetized by using a dose of pentobarbital sodium and the anaesthetized conditions were maintained until the surgical procedure was completed. Anaesthetized animals were prepared for aseptic laparotomy. Aseptic conditions were maintained by using sterile wire and instruments during surgery. Rats were injected with ^{18}F-HAp probes through the tail vein. Abdominal organs were placed *in situ*, and surgical wound was stitched immediately. To ascertain the distribution pattern of the agent, the animals were sacrificed by cardiac

puncture post-anesthesia post-injection. Three animals were used for each time point, collecting main viscera organs (liver, spleen, kidney, lung, muscle and bone).

2 Results and discussion

2.1 Synthesis and TEM characterization

TEM characterization of NPs is one of the most common method. To get good morphology nanoprobe for PET imaging and to check whether F affect the formation of the microcrystals, a large amount of HAp NPs and the trace amount of F-HAp NPs were used for TEM characterization. As shown in Fig.1, the TEM images confirm that the obtained products were typically rodlike shape in nanosize with an average length of 50 nm and an average width of 10 nm. There are no significant difference between them.

To get perfect morphology nanoprobes, three different modifiers were employed for TEM characterization. Fig.2 is the TEM micrographs in the presence of PEG (a), Na-Cit (b) and CTAB (c), respectively. The NPs were irregular and rod-like in the presence of PEG and Na-Cit (Fig.2a, 2b). However,

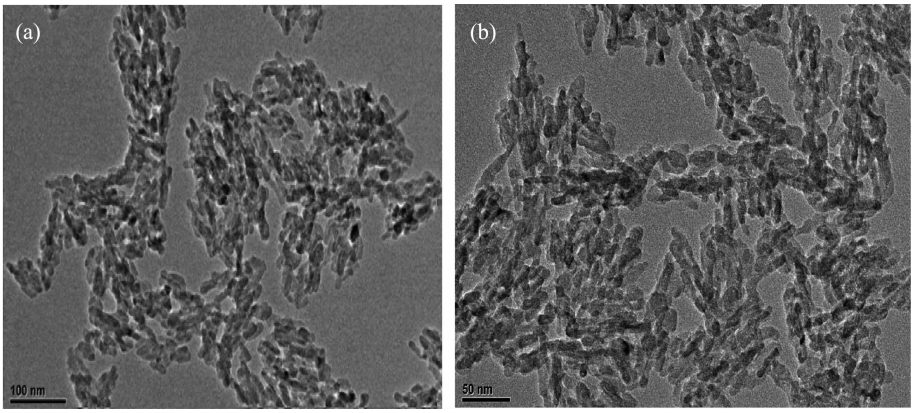

Fig.1 TEM images of HAp NPs in large amounts (a) and trace F doped HAp NPs (b)

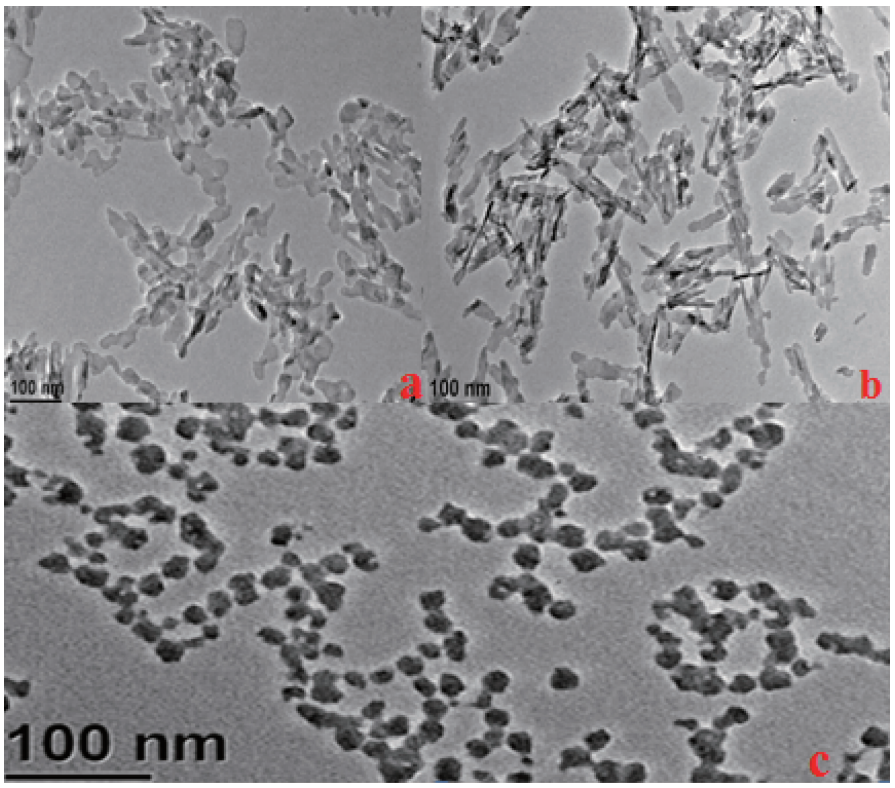

Fig.2 TEM images of PEG (a), Na-Cit (b) and CTAB (c) modified HAp NPs

spherical nanoparticles were formed in the presence of CTAB, with average of 40 nm in diameter(Fig.2c).

As discussed above, citrate molecules actually act as distinct chelating agent, common dispersant and morphology regulator to synthesize morphology-controlled NPs. They also have been extensively used as crystal growth depressant and in a cross-linking role to prepare various size/shape controlled NPs or nanostructures through the route of solution chemistry[26]. Cit^{3-} ligand plays a critical role in the present reaction system, where crystal growth, self-assembly and phase transition coexist. Crystal growth occurred in parallel for the formation of HAp, however, the underlying mechanisms were studied. Chelating ligands of Na-Cit firstly mobilize calcium ions during the first step of starting reagents mixture process to generate Cit-Ca complexes. A citrate molecule has four binding sites, including three COO^- and OH^- group, among which three sites can be bound with Ca^{2+} cations. Ca^{2+} should be first in the form of stable complex owing to efficiently reacting with citrate anions. Upon heating the medium, Ca^{2+} ions are released from the complexes, the supersaturaion condition could be achieved and significantly inhibits the crystal growth. So, when HAp forms, the negative $H_2PO_4^-$, OH^-, and F^- in the solution then react with the free Ca^{2+} to generate F-HAp nuclei. Then, the PO_4^{3-} anions compete with the chelators to produce colloidal sol of HAp, where the HAp nuclei grew into the nanocrystals with covered Cit^{3-} groups, which may selectively bond to certain crystallographic facets of recrystallized HAp via covalent or electrostatic interactions between intramolecular COO^- groups and surface cationic sites Ca^{2+}. With increasing reaction time, these nuclei then grow into big particles along certain orientation due to the selective adsorption of anionic citrate species.

On one hand, Cit^{3-} groups accordingly form a protective layer to hold back the further growth of particles. On the other hand, the noncovalent or weak covalent interactions (*e.g.* electrostatic, hydrogen, coordination bonds) among the surface ligands (OH^- or COO^- groups) stretching outwards of the surface of different nanoparticles probably provide a driving force that makes primary nanounits form monodisperse microspheres. After the complexation of added citric acid to metal ions, the negative charge on the surface of nanoparticles repels each other due to carboxyl groups, preventing agglomeration. Thus, the dispersant can act as a dispersing agent, and the nanoparticles exhibit good monodispersity. It is suggested that upon the above driving force, different HAp NPs move with respect to one another and reach an equilibrium that balance attractions and repulsions, producing a steady state of microspheres with the minimal surface energy. As a result, rod-like HAp NPs appeared.

For PEG, as shown in Scheme 1, when PEG is dissolved in aqueous solution, the PEG-OH bond is formed. PEG molecule has the ability to chelate Ca^{2+}, therefore, PEG-OH can attract Ca^{2+} to form the bond of PEG-O-Ca^{2+}-O-PEG, then PEG-O-Ca^{2+}-O-PEG react with PO_4^{3-} to produce HAp crystal nuclei. In this process, the release rate of Ca^{2+} and PO_4^{3-} are the important factors. The release rate of Ca^{2+} reduced with increasing the concentration of PEG[27]. A large amount of deposits form in a short time when the solution was in the absence of PEG or the concentration of PEG was quite low, indicating HAp produced quickly. With increasing the of PEG, initial deposits were gradually reduced and it required longer time to produce large quantities of deposits, indicating that PEG reduced the release rate of Ca^{2+} and restrained the formation of HAp crystal nuclei. When the release rate of Ca^{2+} and the deposit rate of HAp crystal nuclei depositing in the precipitation center achieve a dynamical equilibrium, HAp crystal nuclei deposit isotropically, and finally the HAp particles are obtained. The HAp crystal nuclei could not deposit isotropically in the precipitation center, so the morphology of as-prepared HAp particles are not spherical.

Surfactant-based systems have been widely used in the synthesis of nanosized materials. CTAB is a typical surfactant controlling particle size, and is used to direct the growth and stabilize the shape of certain types of colloidal nanoparticles[28]. The use of CTAB

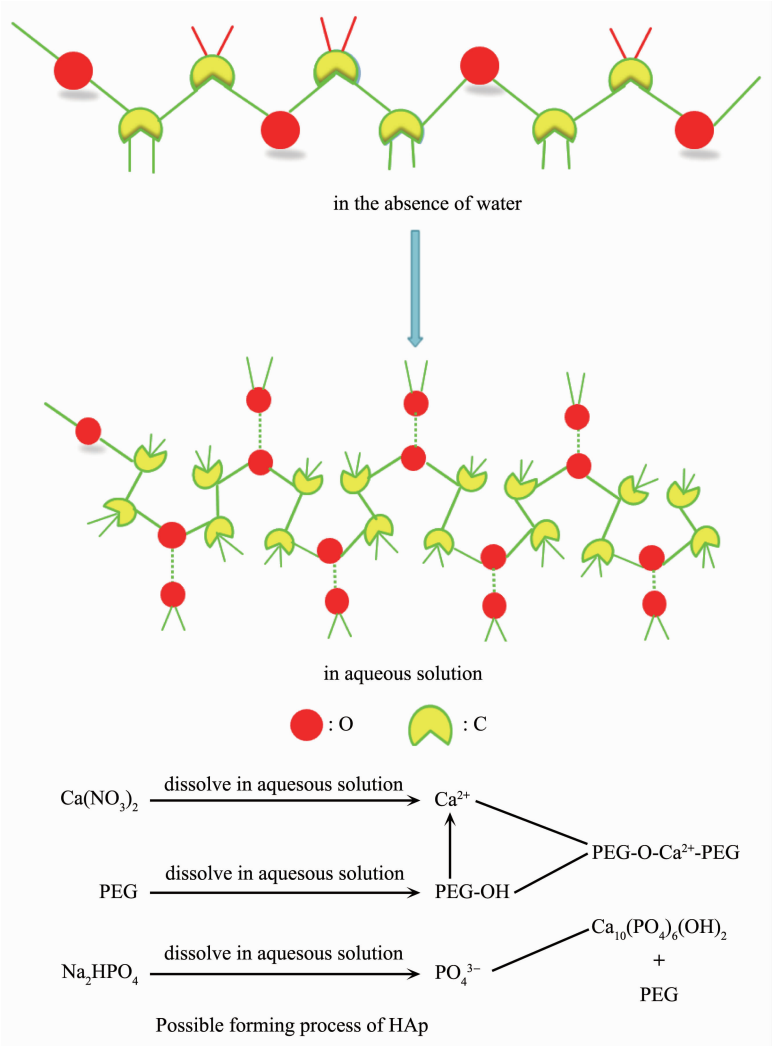

Scheme 1 PEG and schematic illustration of possible forming process of HAp

bases on the theory of critical micelle concentration (CMC). In the presence of CTAB, CTAB might raise the solubility of HAp to some extent and accelerate the dissolution and crystallization process. Since the crystallization process is under CMC, the resulting HAp are invariably nanosphere. The behavior of CTAB is considered to correlate with the charge and stereochemistry properties. In an aqueous system, CTAB would ionize completely and result in a cation with tetrahedral structure. It is then proposed that the charge and structure complementarity endows CTAB with the capability to control the crystallization process. Similar explanation could be made to interpret the experiment of sodium dodecyl sulfonate (SDS). CTAB was an efficient agent for modulating the formation of HAp NPs.

2.2 *In vitro* stability studies

A satisfactory result with stability investigation *in vitro* was obtained. TEM image of rod-shape and sphere-shaped HAp NPs are shown in Fig.3. HAp NPs without CTAB still kept rod shape with a uniform size of 50 nm (Fig.3a). The crystals were spheroidic in shape and well monodisperse with an average size of about 40 nm (Fig.3b) in the presence of CTAB. It is demonstrated that HAp NPs keep stable in PBS.

2.3 EDS characterization

EDS was employed to investigate the elemental composition of HAp. The ^{19}F-doped HAp NPs were characterized instead of ^{18}F-doped. Only Ca, P, and O elements appeared in HAp samples (Fig.4a), corresponding to $Ca_{10}(PO_4)_6(OH)_2$ sample. There was no other element in the sample, excluding carbonaceous

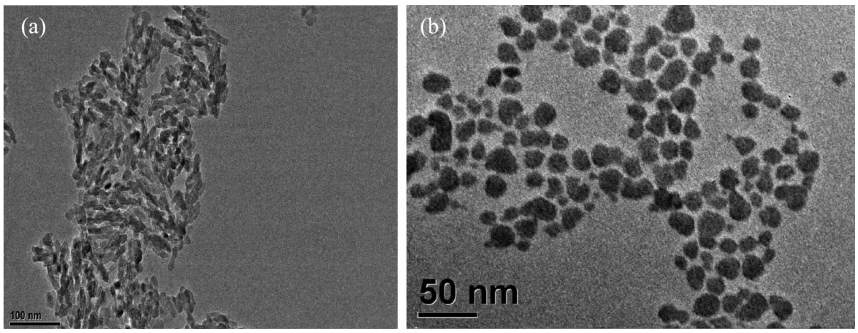

Fig.3　TEM images of HAp NPs with CTAB (b) and without CTAB (a) dispersed in PBS

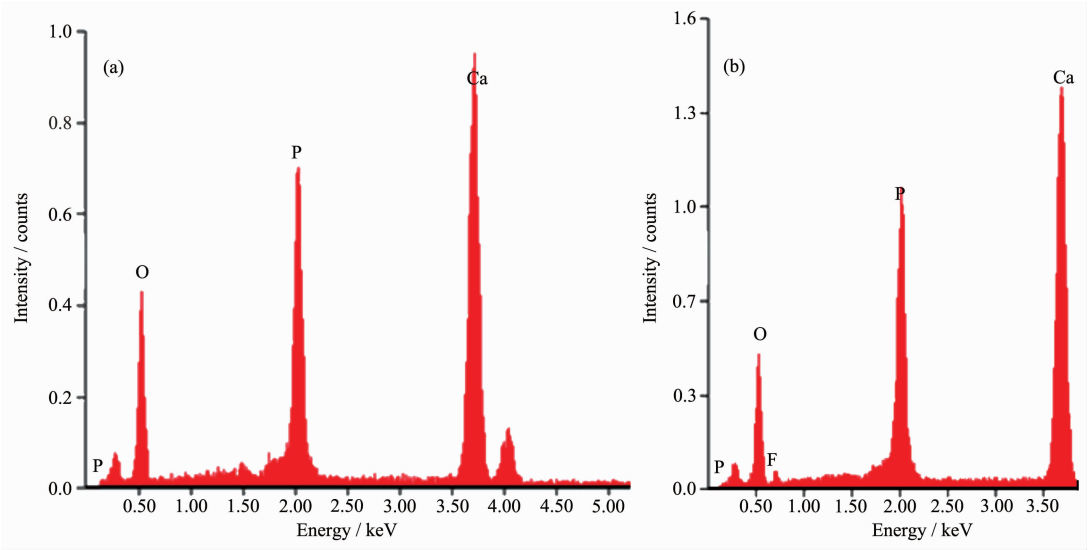

Fig.4　EDS image of HAp NPs (a) and F-HAp NPs (b)

species. The EDS of F-HAp NPs (Fig.4b) depicted the presence of Ca, P, O and F elements. It is indicated that the F element is successful loaded in HAp NPs.

2.4　Mechanism

The mechanism of doping was also explored. The HAp structure with the unconnected PO_4^{3-} tetrahedra orients towards Ca^{2+} ions along the *a*-axis, and the electronegative ions (OH, F, Cl) are placed perpendicularly to Ca^{2+} ions along the *c*-axis, as shown in Fig.5. The hexagonal crystal lattice of apatite is maintained upon the anion substitution. Nevertheless, the different sizes of the ions results in lattice strain, which, in the particular case of F substitution (the ionic radii are 0.168 nm for OH^- and 0.132 nm for F^-) causes a contraction of the *a*-axis. These small structural alterations due to F substitution are probably of crucial importance in the biomineralization mechanism of the apatite containing natural tissues of bones and teeth[29-30].

The radius of fluoride ion is smaller than hydroxyl, so the fluorine ion can replace the position of the hydroxyl groups in the lattice. In addition, the electronegativity of fluorine is larger than oxygen, and the attraction of F-H is stronger than O-H in the hydroxyl groups. So the OH ⋯ F ⋯ OH bond is enhanced. The F-HAp lattice parameters change, and the lattice constant of HAp is larger than F-HAp. The structure arrangement of fluorapatite is more compact

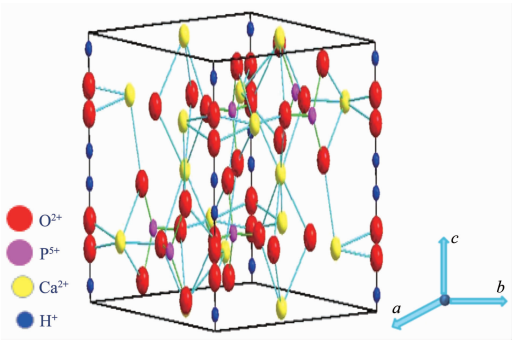

Fig.5　Crystal structure of hydroxyapatite

than hydroxyapatite, and the stability of fluorapatite is better than HAp. As a result, fluorine can be facile to dope in the HAp NPs.

2.5 Radiolabeling yield

To improve density of labeling and get high sensitivity probes, we calculated and evaluated the amounts of ^{18}F labelling theoretically. In addition, it provides a new method to study the amount of labelling in microcosm. Here, the HAp NPs are spherical. Therefore, the volume of each of the NPs can be calculated, and the number of F atom in each nanoparticle was calculated. The results are as follow:

The volume of one HAp crystal cell:

$V_1=0.52\ nm^3$

The volume of one HAp nanoparticle:

$$V_2=\frac{4}{3}\pi r^3=\frac{4}{3}\times 3.14\times 20^3=33\ 493\ nm^3$$

The number of crystal cell in one HAp NP:

$n_1=V_2/V_1=33\ 493/0.52=644\ 10$

The weight of one HAp NP:

$m_1=\rho V=3.16\times 33\ 493\times 10^{-21}=1.06\times 10^{-16}$ g

(The density of HAp is 3.16 $g\cdot cm^{-3}$, the radius of the HAp NP is about 20 nm)

The weight of HAp bases on experiment:

$m_2=50\times 10^{-6}\times 10^{-4}\div 10\times 1\ 004=5.02\times 10^{-7}$ g

(The molar mass of HAp is 1 004 $g\cdot mol^{-1}$)

The total number of HAp NPs:

$m_2/m_1=5.02\times 10^{-7}\div(1.06\times 10^{-16})=4.74\times 10^9$

The total number of HAp crystal cell:

$64\ 410\times 4.74\times 10^9=3.05\times 10^{14}$

As we know, one HAp crystal cell contains two hydroxyl groups. In other words, if the hydroxyl on the HAp were completely replaced by F, one crystal cell has two F, at most.

The number of F atom:

$3.05\times 10^{14}\times 2=6.11\times 10^{14}$

The number of ^{18}F atoms in one nanoparticle:

$6.11\times 10^{14}\div(4.78\times 10^9)=1.28\times 10^5$

For maximum number, there was 1.28×10^5 F atom in one HAp NP. This, however, is only in theory. Actually:

The volume of one HAp NP:

$$V_2=\frac{4}{3}\pi r^3=\frac{4}{3}\times 3.14\times 20^3=33\ 493\ nm^3$$

The calculation formula of weight for radionuclide:

$m=kAMT_{1/2}=2.393\times 10^{-24}\times 1.11\times 10^8\times 18\times 109.8\times 60=3.15\times 10^{-11}$ g

A: radioactivity, 1.11×10^8 Bq; k rely on A: 2.393×10^{-24} mol; M: molar mass of ^{18}F; $T_{1/2}$: half-life, 109.8 min.

So the amount of ^{18}F:

$n_2=3.15\times 10^{-11}/18=1.75\times 10^{-12}$ mol

The number of ^{18}F:

$1.75\times 10^{-12}\times 6.02\times 10^{23}=1.05\times 10^{12}$

The number of ^{18}F atoms in one nanoparticle:

$1.05\times 10^{12}\div 4.78\times 10^9=220$

According to calculation, one HAp NP can label 220 ^{18}F atoms, in theory, which provided robust theory foundation. Fortunately, radiolabeling yield of ^{18}F-HAp determined by measuring the radioactivity associated with the HAp NPs as described in the experimental section was 89% ±0.6%, which was identical with envision.

2.6 Biodistribution studies

The tissue and the organs were excised, and the activity associated with each organs or tissue was measured in counter. The uptake in different organs/tissue was calculated from these data and expressed as injected activity (%). The data revealed that rapid accumulation of 40% was in the liver and 24% in spleen at 30 min. Tibia was considered as the representative of skeleton while calculating total skeleton uptake. Uptake in the bone, muscle, kidney and lung organs were very low (Injected dose fraction per gram <10% ID/g). No appreciable uptake was observed in any of the major organs or tissue, particularly in lungs and spleen, due to the possible leakage of the radiolabeled particulates from liver. Liver and spleen as part of reticuloendothelial system and the colony macrophagocyte, the nanoprobes were facile to target there as well as enhanced permeability and retention effect (EPR). Since free ^{18}F has a native bone targeting capability, the low radioactivity in bone suggests that most of the ^{18}F radiolabels remain intact on HAp NPs. Besides, the weak radioactive signal for the kidney is the evidence of the stability of the ^{18}F-HAp NPs, because metabolism of free ^{18}F passed

through kidney.

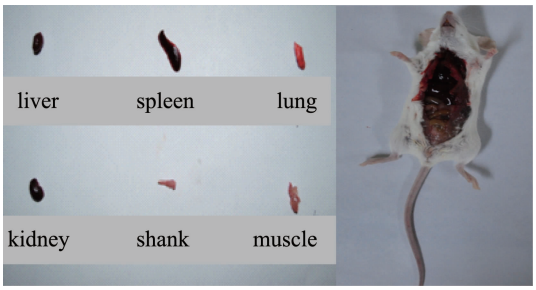

Fig.6　Photos of the organs (A) and vivisectional rat (B)

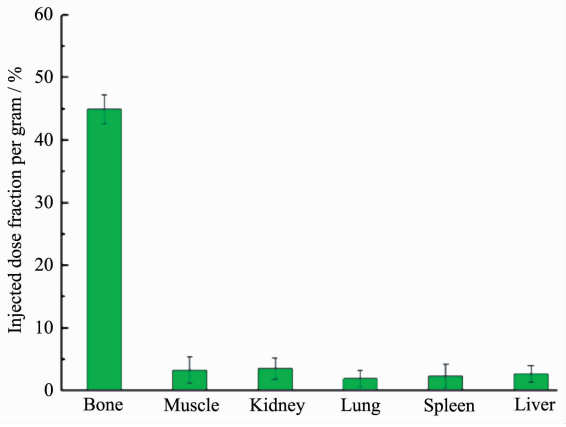

Fig.7　Distribution of free ^{18}F in the rat

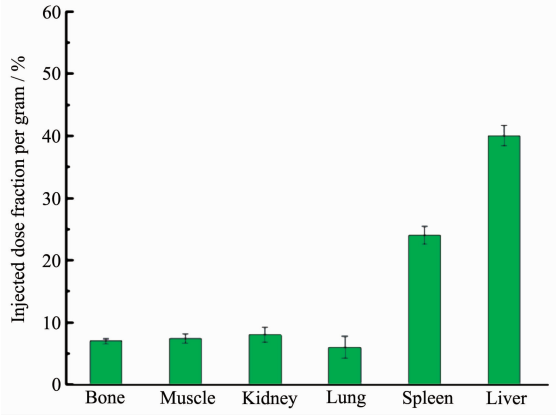

Fig.8　Distribution of ^{18}F-HAP in the body of rat

3　Conclusions

In brief, we have developed a simple, rapid and efficient strategy for synthesis of ^{18}F-labeled HAp. A trace amount of synthesis was employed, with label simultaneously. The method was benefit to improve radiolabeling yield and prevent to leak. The facile ^{18}F-labeling method for HAp NPs will offer significant opportunities for developing molecular image probes. The animal experimentation will open up new perspectives for the preparation of uniform nanoprobes for PET bioimaging application from the cellular scale to whole-body evaluation.

Acknowledgments:

We greatly appreciate the Natural Science Foundation of Shaanxi Province (Grant No.2018JQ2057), Scientific Research Program of Shaanxi Provincal Education Department (Grant No. 17JK0151), PhD Research Foundation Project of Shaanxi University of Technology (Grant No.209020195), National Natural Science Foundation of China (Grant No.21502109), the Key Scientific Research Projects of Shaanxi Education Department(Grants No.18JS023, 17JS027).

Part of this work was performed at Shaanxi Normal University and the General Hospital of Lanzhou Military Region. The authors express their sincere thanks to Jiagen Lv, the professor of Shaanxi Normal University, for his keen interest and constant support. The authors gratefully acknowledge Wansheng Liang. The help rendered by the staff members of the animal house facility of PET-CT center of General Hospital of Lanzhou Military Region is also acknowledged.

References:

[1] Kim D, Lennek P, Dick W S, et al. *Small*, **2009**,**5**:544-557
[2] Cai W B, Chen X Y. *Small*, **2007**,**3**:1840-1854
[3] Tarik F M, Sanjiv S G. *Genes Dev.*, **2003**,**17**:545-580
[4] Markus R, Ralph W. *Nature*, **2003**,**2**:123-131
[5] Wendy R S, Jason H S, Richard C, et al. *Nat. Nanotechnol.*, **2008**,**3**:242-244
[6] Dorothy F, Alper J, Krzystof P, et al. *ACS Nano*, **2010**,**4**:589-594
[7] Heebeom K, Myung S H, Ju R, et al. *Nano Today*, **2011**,**6**:204-220
[8] Evan D N G, Cgyi J S, Caius G R, et al. *Immunol. Rev.*, **2008**,**221**:214-228
[9] Simon M A, Michael H, Pius A S, et al. *Chem. Rev.*, **2008**, **108**:1501-1516
[10]Michae J W, Craig J H, Karen L W, et al. *J. Nucl. Med.*, **2009**,**50**:1743-1746
[11]Neal K D, Edmund J K, Greg M T, et al. *Bioconjugate Chem.*, **2009**,**20**:397-401
[12]Lin Q Y, Sun C G, Li J, et al. *ACS Nano*, **2011**,**5**:3146-3157
[13]Sun Y, Yu M, Liang X S, et al. *Biomaterials*, **2011**,**32**:2999-3007
[14]Sarparanta M, Bimbo L M, Rytknen J, et al. *Mol. Pharmaceutics*, **2012**,**9**:654-660

[15]Xiong L Q, Bin S, Deepak B, et al. *Nanoscale*, **2013**,**5**:3253-3256

[16]Jauregui-Osoro M, Williamson P A, Glaria A, et al. *Dalton Trans*., **2011**,**40**:6226-6237

[17]Elgland M, Nordeman P, Fyrner T, et al. *New J. Chem.*, **2017**,**41**:10231-10236

[18]Dion B, Anna P, Alex J P, et al. *Chem. Soc. Rev.*, **2017**,**46**:4709-4773

[19]Dooraghi A A, Keng P Y, Chen S, et al. *Analyst*, **2013**,**138**:5654-5664

[20]MA Xiao-Yu(马晓雨), LIU Yong-Jia(刘永佳), ZHU Bang-Shang(朱邦尚). *Chinese J. Inorg. Chem.*(无机化学学报), **2018**,**34**(5):917-924

[21]WANG Yan-Hua(王艳华), HAO Hang(郝颃), WU Jian-Xiong(巫剑雄), et al. *Chinese J. Inorg. Chem.*(无机化学学报), **2018**,**34**(8):1517-1530

[22]XU Fu-Qiu(徐伏秋), CHEN Hua-Jun(陈华军), DING Wu-Xiu(丁梧秀). *Chinese J. Inorg. Chem.*(无机化学学报), **2013**,**29**(12):2582-2586

[23]Xu Y J, Dong L, Lu Y, et al. *Nanoscale*, **2016**,**8**:1684-1690

[24]Hui J F, Xiang G L, Xu X X, et al. *Inorg. Chem.*, **2009**,**48**:5614-5616

[25]Hui J F, Wang X. *Chem.-Eur. J.*, **2011**,**17**:6926-6930

[26]Wang Z L, Hao J H, Chan H L W, *J. Mater. Chem.*, **2010**,**20**:3178-3185

[27]He F, Yang P, Wang D. *Inorg. Chem.*, **2011**,**50**:4116-4124

[28]Guan B, Wang T, Zeng S. *Nano. Res.*, **2014**,**7**:246-262

[29]Kannan S, Roch J H G, Agathopoulos S, et al. *Acta Biomater.*, **2007**,**3**:243-249

[30]Basar B, Evis Z. *Mater. Sci. Technol.*, **2009**,**25**:794-798